Smart Structures and Systems, *Vol. 28, No. 4 (2021) 579-592*
https://doi.org/10.12989/sss.2021.28.4.579

Steel dual-ring dampers: Micro-finite element modelling and validation of cyclic behavior

Mahdi Usefvand [1a], Ali Mohammad Rousta [2a], Mojtaba Gorji Azandariani[*3,4a] and Hamid Abdolmaleki [5a]

[1] *Department of Civil Engineering, Maragheh Branch, Islamic Azad University, Maragheh, Iran*
[2] *Department of Civil Engineering, Yasouj University, Yasouj, Iran*
[3] *Centre for Infrastructure Engineering, Western Sydney University, Penrith, Australia*
[4] *Structural Engineering Division, Faculty of Civil Engineering, Semnan University, Semnan, Iran*
[5] *Department of Civil Engineering, Tuyserkan Branch, Islamic Azad University, Tuyserkan, Iran*

(*Received September 16, 2020, Revised June 29, 2021, Accepted July 29, 2021*)

Abstract. Extensive studies have been performed by researchers to increase the ductility and energy-absorption of concentrically braced frames. One of the most widely used strategies for increasing ductility and energy-absorbing is the utilization of energy-dissipation systems. In this regard, the energy-dissipation system consisting of a steel dual-ring damper (SDRD) with different construction details is presented, to improve hysteresis behavior and performance of steel ring dampers (SRD). The most important cause of energy-dissipation in SRDs are the development of bending plastic hinges in the rings. Therefore, by adding an inner ring to the SDR system, it increases the number of moment plastic hinges and in turn increases energy dissipation. Parametric studies havse been performed applying the nonlinear micro-finite element (MFE) procedure to investigate the improved models. The parametric studies comprise examining the efficacy of thickness parameters and the inner ring diameters of the improved models. The SRD models was selected as the base model for comparing and evaluating the effects of improved dampers. MFE models were then analyzed under cyclic loading and nonlinear static methods. Confirmation of the results of the MFE models were performed against the test results. The results indicated that the diameter to the thickness ratio of inner ring of SDRDs has a considerable influence on determining the hysteresis behavior, ductility, ultimate capacity and performance, as well as energy dissipation. Also, the results show that the details of the construction of the internal and external ring connections were a considerable effect on the performance and hysteresis behavior of SDRDs.

Keywords: dual-ring damper (DRD); energy dissipation; micro-finite element (MFE) modeling; performance; yield force

1. Introduction

The energy-absorbing system within the occurrence time of an earthquake absorbs and dissipates a considerable amount of input energy to the structure when it enters the plastic area. Significant economic loss to non-structural and structural elements were observed than the Northridge earthquake in 1994 and the Kobe earthquake in 1995 (Benavent-Climent 2010, Oh *et al*. 2009). In order to lessen the structural and non-structural damages caused by earthquakes, dampers or energy dissipation systems are implemented to control the dynamic response of a structure (Aghlara *et al*. 2018, Duan *et al*. 2019, Hsu and Halim 2018, Qu *et al*. 2019, Rai *et al*. 2013, Sahoo *et al*. 2015, Xu *et al*. 2016, Zhang *et al*. 2012). Energy-dissipation systems were applied in structures in the shape of metallic yielding dampers, friction dampers (Eldin *et al*. 2018, Kori and Jangid 2008), viscoelastic dampers (Farghaly 2015), and viscous fluid dampers (Batterbee and Sims 2005). The metallic yielding dampers are one type of the superlative widely applied energy-dissipation systems with low cost construction and interchangeability. The mechanism of energy dissipation in metallic yielding dampers is through the yield of the damper element and entry into the plastic zone at the time of the earthquake. Dampers also operate as fuse elements that at low and middle seismic levels cause delay entrance of other structural elements into the plastic phase (Bazzaz *et al*. 2012, 2015, Mohammadi *et al*. 2020, Talebizadehsardari *et al*. 2020).

Added damping and stiffness (ADAS) and triangular dampers added damping and stiffness (TADAS) dampers can be mentioned as the most famous dampers that dissipate the energy entering the structure by using bending deformations (Kelly *et al*. 1972, Skinner *et al*. 1974). The ADAS and TADAS members composed of triangular plates placed between the braces and the floor beam, and has the ability to withstand a large number of hysteresis cycles of without resistance deterioration, resulting in is dissipated of large amounts of structural seismic energy (Bergman 1987, Gray *et al*. 2014, Tsai *et al*. 1993, Whittaker *et al*. 1991, Yeh *et al*. 2001). The slit dampers are dissipated the input energy of the earthquake based on the mechanism of flexural plastic deformation (Kim *et al*. 2017). In the field of slit dampers, are can mention the experimental studies of Chan and Albermani (2008) and Li and Li (2007). Also, Oh

*Corresponding author, Ph.D., Professor,
E-mail: m.gorjiazandariani@westernsydney.edu.au; gorji1365@yahoo.com; mgorji@semnan.ac.ir
[a] Ph.D.

ISSN: 1738-1584 (Print), 1738-1991 (Online)

et al. (2009) used slit dampers to improve the seismic performance of beam-to-column connections. Another example of the metallic components of the energy-absorbing is steel shear panels, which the energy entering by the earthquake through the plastic shear deformation of the steel web-plate is dissipated (Chen *et al*. 2013, Rai *et al*. 2013, Xu *et al*. 2016). Nakashima (1995) is provided two the analytical models for evaluating shear panels. In addition to being well-adapted to experimental results, the proposed models were able to predict the decline of strength and strain hardening. Xu *et al*. (2016) tested hysteresis performance of steel shear panels with low-yield-point (LYP) under quasi-static cyclic loading. In these studies, are evaluated cyclic performance, maximum resistance, and hysteresis force-displacement curve of shear panel dampers. Their research shows that LYP steel shear panels have a significant ability to dissipate energy. As a specific kind of metallic dampers, steel pipe dampers (SPDs) were expanded by Maleki and Mahjoubi (2013, 2014) and Maleki and Bagheri (2010a, b), in than energy is dissipated by the shear and flexural plastic hinges. Maleki and Mahjoubi (2014) was presented concrete infilled-pipe damper (CIPD) at the direction improved cyclic behaviour and energy dissipation of SPD. In the following, Maleki and Mahjoubi (2013) was provided steel dual-pipe damper (SDPD) to increase the ultimate capacity, capacity deformation or ductility, and modifying the force-displacement hysteresis curve of SPD. In SDPDs by shear and axial deformations is dissipated energy. The energy dissipation of SDPDs is occurrs in short displacements by the pipe shear force and in great displacements by the pipe axial force. The results of experiments and numerical investigates indicate that the dampers of the pipe display well ductility, high energy absorption and stability cyclic behaviour.

The idea using ring damper (RD) in the beam-to-column connection was provided by Koetaka *et al*. (2005). The results of studies of Koetaka *et al*. (2005) shows that of a ring damper increases the performance and energy dissipated in the beam-to-column connections under cyclic loading. Abbasnia *et al*. (2008) based on the proposed ring damper by Koetaka *et al*. (2005), suggested the idea of using a steel ring as a flexible/fuse element at the end of the brace members in the concentrically braced frame (CBF) systems. Abbasnia *et al*. (2008) showed that, the ring damper member not only dissipates energy properly, but also prevents out-of-plane deformation the brace member. The hysteresis behavior and performance of steel RDs were examined applying the experimental and finite element method by Andalib *et al*. (2014). Gorji Azandariani *et al*. (2020a, b) investigated the cyclic performance of steel ring dampers in CBFs systems in analytical and finite element approaches. The proposed analytical relationship by Gorji Azandariani *et al*. (2020a, b) have predicted the yielding force, yielding displacement, and initial stiffness of steel ring with good precision. Also, the comparison between the steel RDs and other metallic dampers are exhibited well seismic performance and excellent energy dissipation. The results of investigates on steel ring dampers as energy-absorbing and fuse/flexible members in CBFs systems, were demonstrated their well flexibility, energy absorption, and stability cyclic behaviour (Abbasnia *et al*. 2008, Andalib *et al*. 2014, Gorji Azandariani *et al*. 2020a).

The results of investigating the cyclic behavior of steel RDs in concentrically braced frames (CBFs) systems, exhibited well ductility, high energy dissipation, and stable load-displacement loops (Gorji Azandariani *et al*. 2020a, b). The aim of references (Abbasnia *et al*. 2008, Andalib *et al*. 2014) was investigating the cyclic behavior and energy dissipation of the steel RDs. In this study, in order to improve the seismic performance of steel RDs, use has been made of steel dual-ring dampers (DRDs) with very low construction costs. This investigate aims to improve the hysteresis behavior and increment of the capacity and energy-dissipation of the steel RDs, as well as to prepare the micro-finite element (MFE) model to assessment the ductility parameter and failur mode of the steel DRDs with different construction details.

The use of metallic yielding dampers in the improvement and strengthening of structures as well as the control of floor displacement has always been considered by researchers. On the other hand, low construction costs and easy interchangeability are some of the most important issues in providing a new damper. Despite the introduction of numerous metallic yielding dampers, energy-absorbing systems are still provided and developed. Steel ring dampers are among the new dampers with low construction costs and easy interchangeability. Studies performed by Abbasnia *et al*. (2008), Andalib *et al*. (2014) and Gorji Azandariani *et al*. (2020a, b) are limited to examining the cyclic behavior and energy absorption of steel ring dampers. Results of studies on SRDs as ductile and energy-absorbing elements in concentrically bracing systems showed good ductility, energy dissipation, and stable hysteresis loops. These investigations experimental were limited to a few test specimens and fixed geometry and details for the ring dampers. The aim of Refs. Gorji Azandariani *et al*. (2020a, b) were to investigate the cyclic behavior and energy absorption of the steel ring dampers and steel dual-ring dampers. Given the studies performed by the Refs. (Abbasnia *et al*. 2008, Andalib *et al*. 2014, Gorji Azandariani *et al*. 2020a), this research aims to proposed dual-ring steel dampers to improve the performance of the steel ring dampers, as well as evaluate and compare three types of dampers (i) steel ring damper, (ii) steel dual-ring damper with horizontal and vertical connection plate between two rings, (iii) steel dual-ring damper with X-shaped connection plate between two rings. The micro-finite element (MFE) model was developed to evaluate the ductility parameter and failure state of steel ring dampers as well as validation with experimental results. Also, extensive parametric studies were performed to evaluate and compare the proposed dual-ring dampers with ring dampers.

In this research, the behavior and performance of steel dual-ring dampers (DRDs) with different construction details have been investigated by micro-finite element (MFE) methods. The steel dual-ring dampers (DRDs) using MFE methods have been expanded applying package ABAQUS (2010) software. In this study, have been making

parametric studies in order to examine the effects of construction different on cyclic behavior and the performance of steel DRDs. The target of parametric studies is to examine and appraise the initial stiffness, yielding force, displacement ductility, and energy dissipation of steel DRDs, as well as the mechanism of plastic hinge formation during the collapse.

2. Micro-finite element modeling

In order to investigation the behavior of the steel DRDs, an impressive and precise micro-finite element method is incorporated. All the modelling steps are provided as follows:

2.1 Geometry and details of the test specimens

In this section, using the test results (Abbasnia *et al*. 2008, Andalib *et al*. 2014) and data, use has been made of ABAQUS software to examine the hysteresis behavior of steel DRDs more accurately (ABAQUS 2010). Micro-finite element modeling was performed using ABAQUS and were examined the load-displacement curves and damage shapes of the computational and experimental samples. To achieve this objective, the W1, W2, and W3 test samples from Andalib *et al*. (2014) and CT20 test sample of Abbasnia *et al*. (2008) were selected and applied for MFE modelling. The geometry and configuration of test samples of Abbasnia *et al*. (2008) and Andalib *et al*. (2014) are given in Fig. 1. According to Fig. 1, the thickness and diameter of the ring with similar specifications are 12 mm and 220 mm, respectively. Also, the ring length of CT20 specimen was 100 mm and for W1, W2 and W3 specimens was 150 mm. The CT20 experimental sample was made of a steel ring welded to the connection of two gusset plates. For making W1, W2, and W3 experimental specimens, used was made of two mid-rings with two connection plates. The steel plate with 12×150×220 mm dimensions is used to make the mid-ring, and the steel plate connection has dimensions of 20×250×400 mm. For this purpose, eight F20 screws were used to connect the mid-rings to the connections plates (Fig. 4).

2.2 Materials properties

The cyclic constitutive model has been known to modelling the hysteretic behavior identically (Shi *et al*. 2011), which was presented by Chaboche (1986, 1989), including an nonlinear isotropic hardening and kinematic hardening components. The kinematic and isotropic hardening combination plasticity model is applied to modelling the hysteresis behavior of the steel material (*J2 material*). This model is available in ABAQUS software as a tool in the materials section, which is parameterized as (*Hardening*: *Combined*; *Data type*: *Stabilized model*). The input parameters in this model are in the feature of stress-strain data obtained from the experiment, also the ideal multi-line graph is in accordance with the stress-strain diagram of the test. References (Abbasnia *et al*. 2008, Gorji Azandariani *et al*. 2020b) exhibited that the multi-linear stress-strain curve used for the steel under cyclic loading has a good accuracy. Therefore, in the modeling process, it is assumed that the stress-strain curve of the steel is the ideal multi-linear, as shown in Fig. 2.

The elastic zone of properties of steel material the Poisson's coefficient and modulus of elasticity values were, 0.3 and 200 GPa, respectively. Also, for the hardening region, the nonlinear isotropic and kinematic hardening combination law is adapted (Gorji Azandariani *et al*. 2020a, b). The nominal yield and ultimate tensile strength steel values employed in the analysis for CT20 of Ref. (Abbasnia *et al*. 2008) 305 Mpa and 480 MPa, respectively, have been adopted. Also, the nominal yield and ultimate tensile

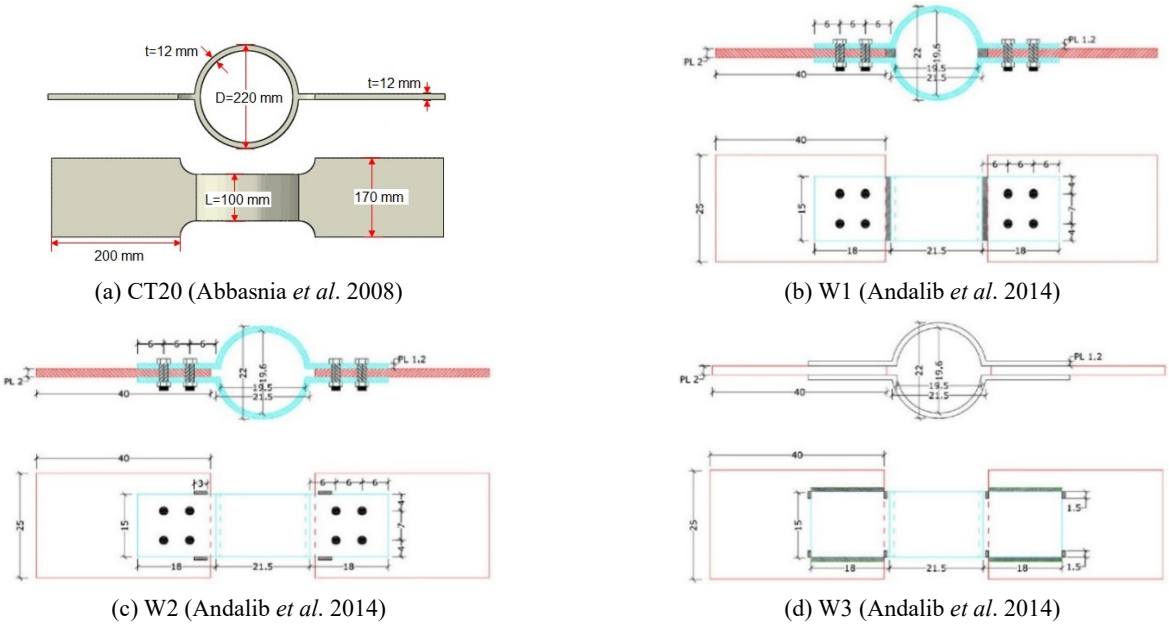

(a) CT20 (Abbasnia *et al*. 2008)

(b) W1 (Andalib *et al*. 2014)

(c) W2 (Andalib *et al*. 2014)

(d) W3 (Andalib *et al*. 2014)

Fig. 1 Dimensions and geometry of the test samples

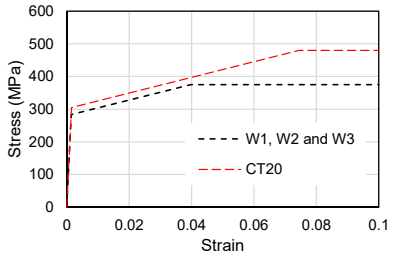

Fig. 2 Stress-strain curve applied in the MFE modelling

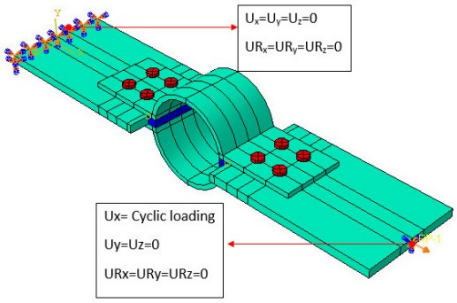

Fig. 3 Boundary conditions and loading of MFE models

strength steel values employed in the analysis for models W1, W2 and W3 of Ref. (Andalib *et al*. 2014) 283 Mpa and 375 MPa, respectively, have been adopted.

2.3 Boundary conditions and cyclic loading

In the micro-finite element models, the boundary conditions and cyclic loading considered are according to the experimental setup (Abbasnia *et al*. 2008, Andalib *et al*. 2014). According to the experimental setup (Abbasnia *et al*. 2008, Andalib *et al*. 2014), Fully restrained boundary condition is applied to one end of the model while a cyclic loading of displacement type is exerted on the other end, to assess the cyclic behavior of the steel ring damper models. The restrained endplate and the location of the cyclic loading are shown in Fig. 3. Cyclic loading is applied along the longitudinal side of the connection plate and is fixed at other locations to prevent out-of-plane loading (Fig. 3). The cyclic loading protocol was applied to micro-finite element models based on ATC-24 (1992). For the interaction between parts, the tangential and normal behaviors were considered in the modelling of the contact interactions. For the tangential behavior, the coefficient of friction is taken equal to 0.3 and for the normal behavior the *Hard Contact* type is considered (AISC 2016, Vilela *et al*. 2019).

2.4 Meshing and method of analysis

A typical steel ring damper commonly contains a steel ring, gusset plates, bolts, and welds, as exhibited in Fig. 1. For this purpose, 3D elements were used for the modelling and solid elements were employed to model the ring damper, gusset plates, welds and bolts. Solid elements (*Hex-structure*: *C3D8R*) (ABAQUS 2010), that is an 8-node isotropic three dimensional element with reduced integration, has been used for meshing. The configuration and meshing

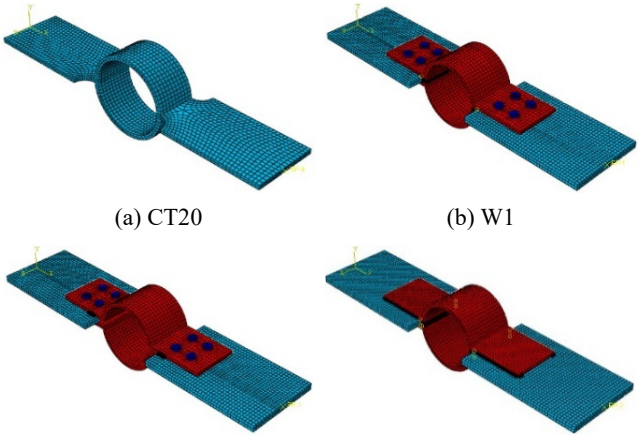

(a) CT20 (b) W1

(c) W2 (d) W3

Fig. 4 Configuration and meshing of the MFE models

of the MFE models are illustrated in Fig. 4. In the MFE modelling of the geometry and materials non-linear behaviour, the impact of strain hardening and great displacement on the solid elements of the report is considered. In the analysis of the MFE models the implicit technique (*Nonlinear General Static*) (ABAQUS 2010) and Newton-Raphson procedure (Mohebkhah and Azandariani 2016) were utilized. According to the sensitivity analysis results of meshing, the dimensions of 10×10 are specified for meshing, which satisfy the necessary computational precision. Furthermore, Hex structural meshes are implemented for modelling. The incremental time step measure is computed automatically in ABAQUS, based on the models' minimize mesh dimensions.

3. Validation of MFE models

The results of experiments examined by Abbasnia *et al*. (2008) and Andalib *et al*. (2014) were used for confirmation of the MFE models precision. The MFE modeling methodology, meshing and approach of analysis, materials properties, interactions, loading and boundary conditions are provided in Sec. 2. To confirmation numerical models, were examined the load-displacement curves and damage shapes of MFE models and experimental samples (Abbasnia *et al*. 2008, Andalib *et al*. 2014). In Table 1, the models' dimensions, as well as the maximum compressive and tensile loads of the MFE models and the test (Abbasnia *et al*. 2008, Andalib *et al*. 2014) resultsare provided. Eq. (1) was applied to evaluate the error ratio of the MFE models with respect to the test results. Conforming to Table 1, the mean error of MFE models and test specimens using Eq. (1) is 1.8%. In the MFE models was observed that have appropriately evaluated the maximum compressive and tensile loads of the steel RD.

$$Error\ (\%) = \frac{\left|P_{Max}^{Exp} - P_{Max}^{FEM}\right|}{P_{Max}^{Exp}} \times 100 \qquad (1)$$

Hysteresis load-displacement results of the micro-finite elements steel ring dampers under cyclic loading are

Table 1 Test results and MFE models predictions of the maximum load

Tested by	Spes.	Dims. of rings (mm)			Max. Load(EXP)		Max. Load(FEM)		Error%
		t	D	L	Tension (kN)	Compression (kN)	Tension (kN)	Compression (kN)	
Andalib *et al.* (2014)	W1	12	220	150	120.7	103.5	120.5	103.3	0.2
	W2	12	220	150	118.2	83.7	122.7	81.6	3.2
	W3	12	220	150	117.6	100.8	120.1	95.5	3.7
Abbasnia *et al.* (2008)	CT20	12	220	100	87.7	73.7	87.6	73.4	0.3
Mean									1.8

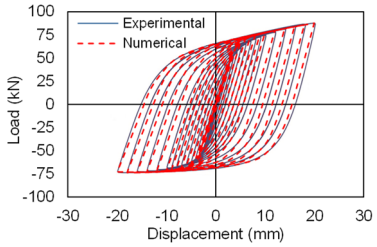

(a) CT20

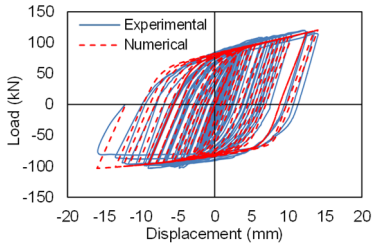

(b) W1

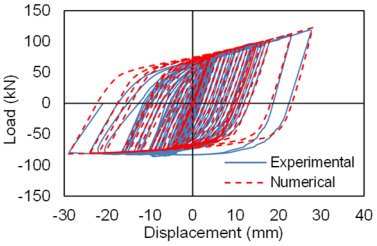

(c) W2

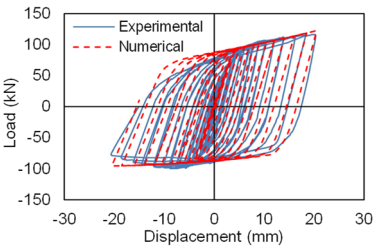

(d) W3

Fig. 5 Comparison between the test (Abbasnia *et al*. 2008, Andalib *et al*. 2014) and MFE models hysteresis curves

displayed in Fig. 5. Also, in Fig. 5 were exhibited the hysteresis force-displacement of the experimental tests (Abbasnia *et al*. 2008, Andalib *et al*. 2014) to compare them

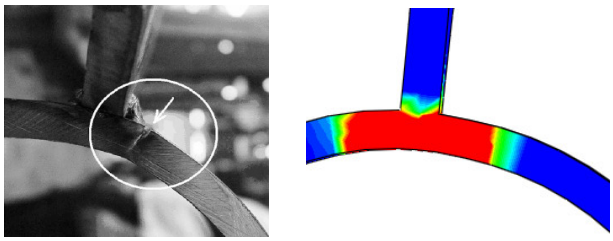

(a) CT20

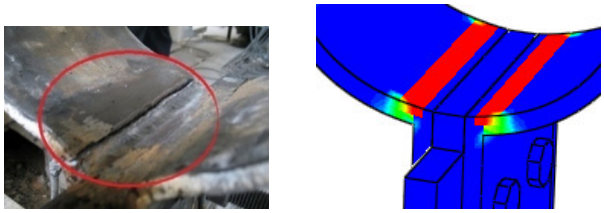

(b) W1

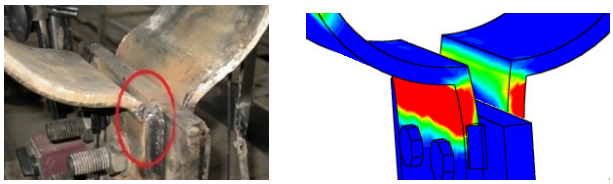

(c) W2

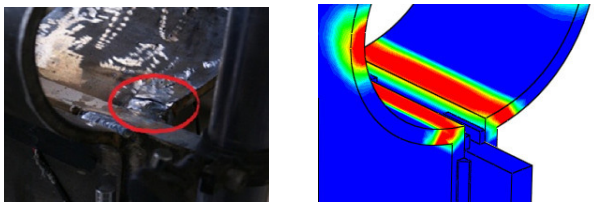

(d) W3

Fig. 6 Comparison between the test (Abbasnia *et al*. 2008, Andalib *et al*. 2014) and MFE models failure modes

with the results of the MFE models. The comparison of the hysteresis force-displacement curve demonstrates that the MFE models predict the hysteresis force-displacement, stiffness, and maximum load of the test samples with a qualified precision.

In Fig. 6, were illustrated comparison the damage shapes of the MFE models and the test samples (Abbasnia *et al*. 2008, Andalib *et al*. 2014). Equivalent plastic strain (PEEQ) was applied to measure the damage regions in MFE

models. In Fig. 6, the damage regions of the samples tested by Abbasnia *et al*. (2008) and Andalib *et al*. (2014), as well as the PEEQ of MFE models for are exhibited for comparing with the test specimens. The most PEEQ occurred at the steel ring to plate connection, which are according to with the experimental results.

4. Developing an improved model for the steel ring damper

Several studies have been performed by the researchers using the experimental and numerical methods in order to provide strategies for improving the performance of active and passive energy dissipation systems in buildings. On the other hand, passive energy-absorbing systems have received attention due to the stable behavior of the hysteresis loops and quick and interchangeable installation process. Many of these energy-absorbing systems are proposed to improve seismic behavior and energy absorption in concentrically braced frame systems. One of the disadvantages of concentrically braced frame systems is brace buckling in the compression state, which has a significant impact on reducing capacity, ductility, and energy absorption. Therefore, energy-absorbing systems have been provided by researchers to improve the performance of braces in concentrically braced frame systems. For the chevron bracing system examples of the energy dissipation systems are ADAS and TADAS (Bergman 1987, Gray *et al*. 2014, Tsai *et al*. 1993, Whittaker *et al*. 1991, Yeh *et al*. 2001), steel ring dampers (Abbasnia *et al*. 2008, Andalib *et al*. 2014, Gorji Azandariani *et al*. 2020a, b), low-yield-point steel panels dampers (Rai *et al*. 2013, Xu *et al*. 2016), and pipe dampers (Mahjoubi and Maleki 2016, Maleki and Bagheri 2010a, b, Maleki and Mahjoubi 2013, 2014). Also, for the diagonal bracing system one could mention the curved dampers (Hsu and Halim 2018, 2017, Zhou *et al*. 2019), shear-moment metal dampers (Sahoo *et al*. 2015), and buckling restraint brace (BRB) system (Li *et al*. 2019, Wang *et al*. 2019). The energy damping systems provided are suitable for diagonal bracing with stable hysteresis behavior and energy absorption but are not cost-effective in terms of construction and interchangeability. Due to the axial behavior of the diagonal bracing, the use of a steel ring damper with bending behavior was suggested to improve the performance of the bracing system (Abbasnia *et al*. 2008, Andalib *et al*. 2014, Gorji Azandariani *et al*. 2020a, b). In concentrically braced frame systems, the ductile steel RD is connected to the end of the brace member to enhancement the ductility and to prevent damage to the compression member. It also has the advantage of economic installation and replacement after damage. Studies performed on the steel RDs are bounded to investigating the hysteresis behavior and energy-dissipation and have presented analytical relationships for estimating their ultimate capacity. The investigation on steel ring dampers as ductile and energy-dissipation elements in CBF systems exhibited well ductility, high energy dissipation, and stability behavior in the force-displacement curve. The application of steel RDs in controlling seismic response of structures, as well as increase of the energy absorption in CBFs systems have been more under focus of attention. The configuration and placement of the steel RDs in the CBF systems are exhibited in Fig. 7. According to exhibited in Fig. 7, the steel RD is connected between the brace end and the gusset plate connection.

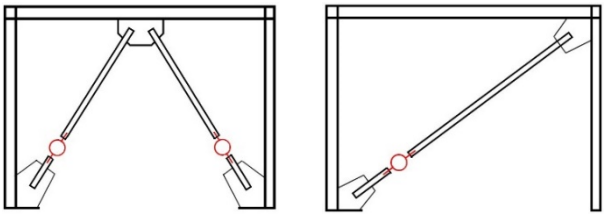

Fig. 7 The configuration and placement of the steel RDs in the CBF systems

In this study, the steel DRDs are presented to improve the behavior and performance of the steel ring damper. The steel DRDs are made of dual concentric rings which are linked to each other by connection steel plates. In order to evaluate the hysteresis behavior of the proposed improved models, the experimental sample of the steel ring tested by Abbasnia *et al*. (2008) was selected as the base model. The geometries of the selected base model and improved models are shown in Fig. 8. Improved models were developed based on the basic model for parametric studies. The improving strategies are investigated as follows:

4.1 Steel ring damper (*SRD*)

In this model, the base model is identical with the validation model of tested specimen by Abbasnia *et al*. (2008). The thickness, length, and mean diameter values of the ring were considered 12, 100, and 208 mm, respectively (Fig. 8(a)).

4.2 Steel DRD with horizontal connection plate between two rings (*SDRDH*)

This model was developed by adding an inner ring to the base model. Then the inner and outer rings were connected to each other using the horizontal connection plates (Fig. 8(b)). The thickness, length, and mean outer diameters for the ring were 12, 100, and 208 mm, respectively. The diameter and thickness of the inner ring have been considered as a variable parameter.

4.3 Steel DRD with cruciate connection plate between two ring (*SDRDC*)

This model was developed by adding an inner ring to the base model, and by connecting the inner and outer rings to each other using the vertical and horizontal connection plates (Fig. 8(c)). The thickness, length, and mean outer diameters for the ring were 12, 100, and 208 mm, respectively. The diameter and thickness of the inner ring have been considered as a variable parameter.

4.4 Steel DRD with X-shaped connection plate between two ring (*SDRDX*)

This model was developed by adding an inner ring to the base model, and by connecting the inner and outer rings

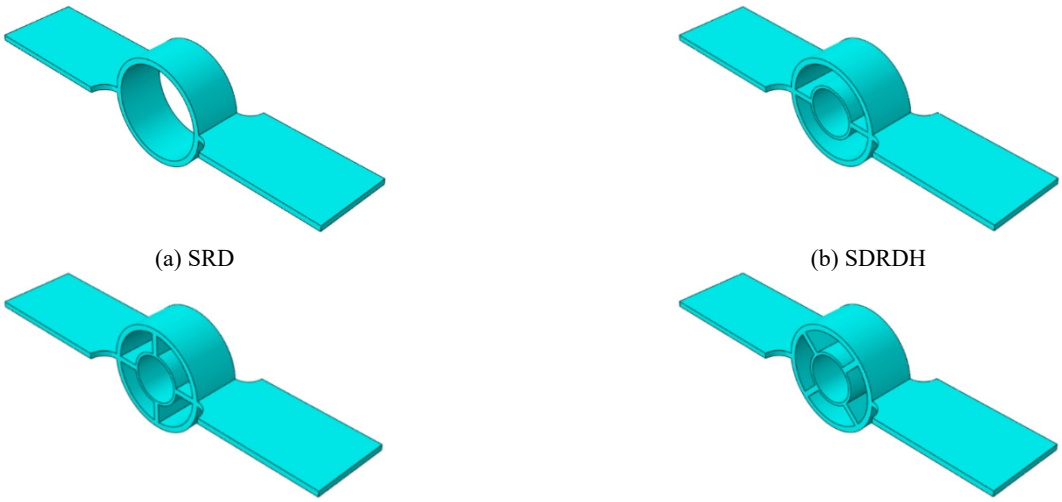

(a) SRD (b) SDRDH

(c) SDRDC (d) SDRDX

Fig. 8 Adopted improved models for the steel rings damper

to each other using the X-shaped connection sheets (Fig. 8(d)). The thickness, length, and mean outer diameters for the ring were 12, 100, and 208 mm, respectively. The diameter and thickness of the inner ring have been considered as a variable parameter.

5. Parametric study

The final aim of this study was providing a micro-finite element improved model for a steel ring damper, and applying its results for the future research. Hence, the steel dual-ring damper is implemented, which consists of two concentric steel made rings. For connecting the internal and external rings, three manufacturing strategies have been incorporated, which are mentioned in Section 4. Therefore, parametric studies have been made to investigate the effects of inner ring thickness and type of the ring connections to each other, on the hysteresis behavior and performance of steel DRD. The MFE improved models at the parametric studies were expanded according to the test sample of Abbasnia *et al*. (2008). In this section, first the parametric models are introduced and the geometric details, loading and properties of the materials are presented. Also, in continuation, the general results of the models are presented.

5.1 Specifications of models

The details and dimensions of configurations of the investigated ring damper and improved models are exhibited in Fig. 9 and their cross-sectional dimensions, mean diameter, thickness and length of inner and outer rings are presented in Table 2. Conforming to Fig. 9, the specifications investigated in these parametric studies contained the thickness of inner ring (t_i) and inner ring diameter (D_i). The length of the outer and inner ring (L) is constant, as exhibited in Fig. 9, amount is assumed to be 100 mm. The diameter of the inner ring (D_i) has been taken equal to 108, 106, 104, 102, and 98 mm. the Diameter (D_o) and thickness (t_o) of the outer ring are fixed and equal to 208 and 12 mm, respectively (Table 2). The diameter to thickness of the inner ring (D_i/t_i) for parametric studies were selected equal to 54.0, 26.5, 17.3, 12.7, and 8.1. Also, the diameter to thickness of the outer ring (D_o/t_o) for ring damper and improved models was considered as 17.3. Therefore, the dimensionless variable parameter, α, which is obtained from the ratio of D_o/t_o to D_i/t_i, is utilized to examine the impacts of inner ring thickness and diameter. Accordingly, the values of parameter α are considered equal to 0.32, 0.65, 1.00, 1.36 and 2.12. The abbreviation names and configuration of the dimensions of the ring damper and improved models are provided in Table 2. The SRD, SDRDH-α, SDRDC-α, and SDRDX-α abbreviation have been applied to name the ring damper and improved models. The materials characteristics used in the parametric studies have been adopted from the test data of Abbasnia *et al*. (2008). The nominal yielding and ultimate tensile strength of steel utilized in the analysis were 305 MPa and 480 MPa, respectively, for the parametric models. Also, for the elastic zone of properties of steel material the Poisson's coefficient and modulus of elasticity values were, 0.3 and 200 GPa, respectively. In the modeling of materials, the elastic-plastic hardening (*EPH*) stress-strain curve was considered (Gorji Azandariani *et al*. 2020a). The support conditions and cyclic loading procedure of parametric models, were adopted from the test specimens of Abbasnia *et al*. (2008). The loading protocol for displacement control has been considered in conformity to ATC-24 (1992) for cyclic analysis of the micro-finite element models.

5.2 Results of ring damper and improved models

The ring damper and improved models are analyzed under cyclic loading and the results are reported in Table 3. The results of the analysis of models contained the initial stiffness, yielding displacement, yielding force, ductility, and cumulative energy dissipation, as well as yield force to weight ratio (FWR). The initial stiffness, yield displacement, and yield force are computed conforming to the

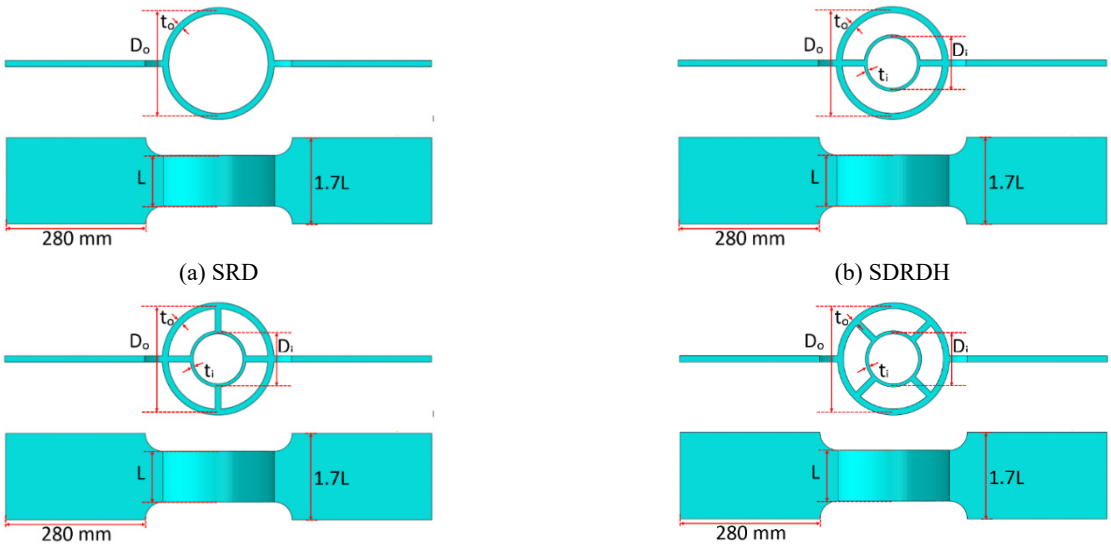

(a) SRD (b) SDRDH

(c) SDRDC (d) SDRDX

Fig. 9 Details and dimensions of MFE models

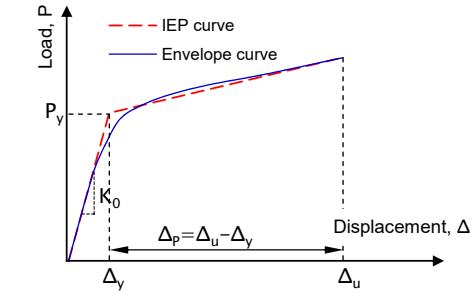

Fig. 10 Envelope and equivalent bilinear curve

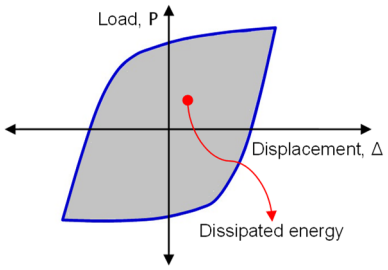

Fig. 11 The energy dissipation based on the hysteresis loop

Table 2 Dimensions and results of the ring damper and improved models

Model-α	Dimensions of rings (mm)						$\alpha = \frac{D_o/t_o}{D_i/t_i}$	K_0 (kN/mm)	Δ_y (mm)	P_y (kN)	μ^a (Δ_u/Δ_y)	E_D (kJ)	FWR[b] (KN/kg)
	D_o	D_i	t_o	t_i	D_o/t_o	D_i/t_i							
SRD		-		-		-	-	15.73	4.34	68.3	4.61	18.8	11.1
SDRDH-0.32		108		2		54.0	0.32	14.21	4.59	65.2	4.36	17.8	8.5
SDRDH-0.65		106		4		26.5	0.65	16.63	4.11	68.3	4.87	19.5	8.4
SDRDH-1.00		104		6		17.3	1.00	39.68	2.45	97.0	8.19	37.3	11.2
SDRDH-1.36		102		8		12.7	1.36	76.86	2.10	161.0	9.55	65.2	17.5
SDRDH-2.12		98		12		8.1	2.12	113.58	1.96	222.7	10.21	87.0	22.0
SDRDC-0.32		108		2		54.0	0.32	16.65	4.30	71.5	4.66	19.9	8.3
SDRDC-0.65	208	106	12	4	17.3	26.5	0.65	16.95	4.05	68.5	4.95	19.9	7.5
SDRDC-1.00		104		6		17.3	1.00	40.40	2.64	106.6	7.58	39.6	11.0
SDRDC-1.36		102		8		12.7	1.36	72.90	2.29	166.9	8.73	64.9	16.4
SDRDC-2.12		98		12		8.1	2.12	117.47	2.18	255.5	9.20	96.0	22.9
SDRDX-0.32		108		2		54.0	0.32	19.78	6.95	137.4	2.93	26.3	16.0
SDRDX-0.65		106		4		26.5	0.65	25.78	5.75	148.1	3.52	30.4	16.2
SDRDX-1.00		104		6		17.3	1.00	32.22	5.75	185.2	3.52	38.1	19.2
SDRDX-1.36		102		8		12.7	1.36	87.65	2.35	205.7	8.52	75.5	20.2
SDRDX-2.12		98		12		8.1	2.12	86.10	2.36	203.3	8.48	75.8	18.2

[a] Ductility
[b] Yield force to weight ratio (FWR)

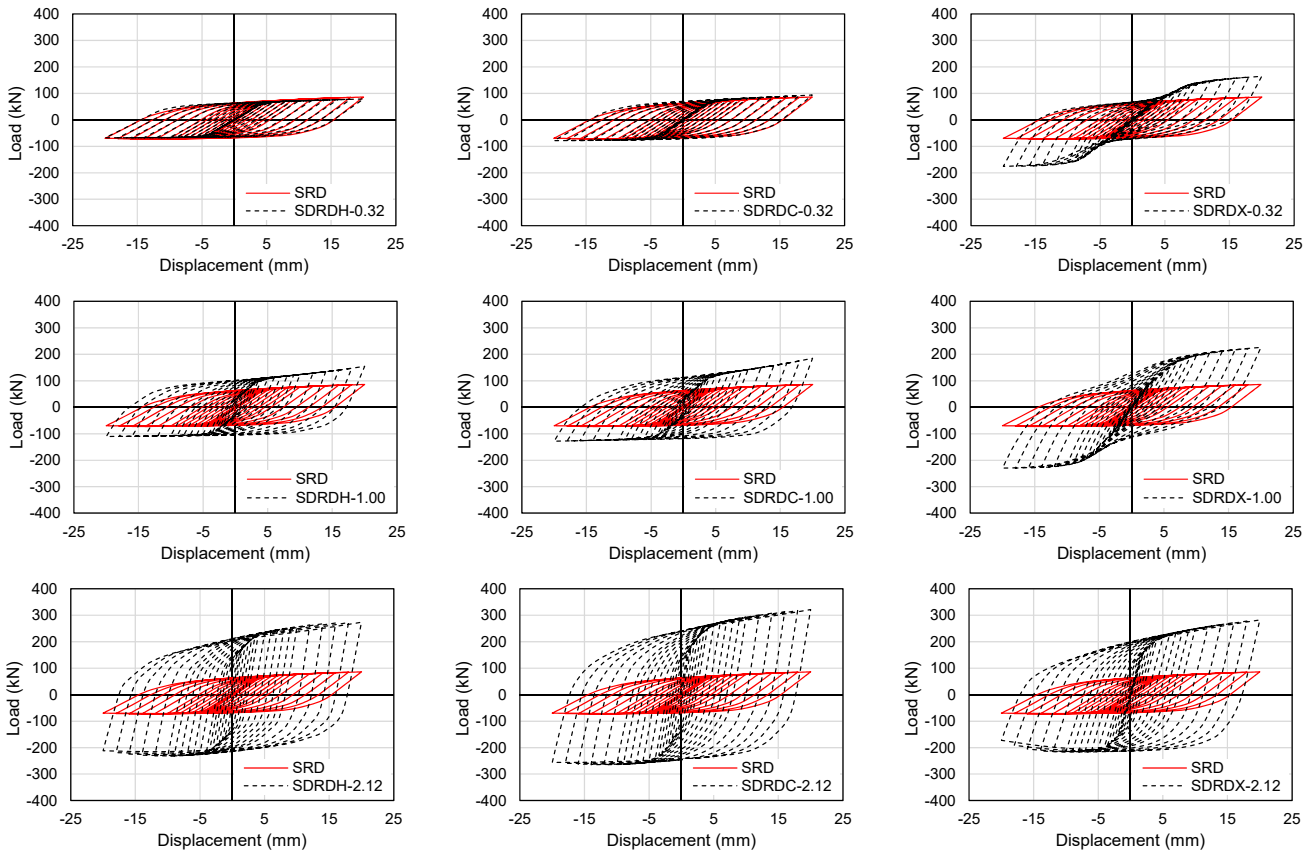

(a) SDRDH (b) SDRDC (c) SDRDX

Fig. 12 Comparison of hysteresis curves of the improved models with SRD

equivalent idealized elastoplastic (IEP) curve for envelope curve is adopted by the FEMA-356 (2000) (Fig. 10). To calculate the energy dissipation, the enclosed surface inside the hysteresis loops is utilized. Fig. 11 shows a hysteresis ring and its illustrated area, which is equal to the dissipated energy in this cycle. The cumulative energy dissipation is obtained the aggregate of the total area surrounded the hysteresis loops of the force-displacement curve. The ductility parameter for models has been calculated from the maximum displacement ratio to the yield displacement obtained from the IEP curve. Another parameter obtained from the results of parametric models is the force to weight (FWR) ratio. This parameter is selected to determine the model and the optimal ratio of the diameter to inner ring thickness.

6. Performance of the improved dampers

6.1 Cyclic and global behavior

In Fig. 12, the hysteresis curves of the micro-finite element models present in Table 2 are shown. To compare the hysteresis curves, the improved models with the base model (i.e., the steel ring damper (SRD)), are shown in Fig. 12 together with the hysteresis curves of the base model and the improved models. Figs. 13 and 14 illustrate the comparison between the envelope curve and cumulative dissipated energy of the parametric models. By comparing the hysteresis and envelope curves of the parametric models in Figs. 12 and 13, for values of $\alpha < 1$ in the improved models SDRDH and SDRDC, the cyclic behavior is similar

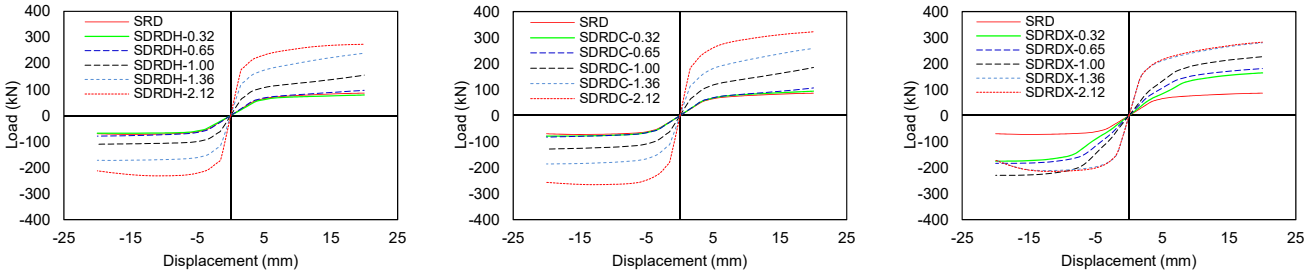

(a) SDRDH (b) SDRDC (c) SDRDX

Fig. 13 Comparison of envelope curves of the parametric models

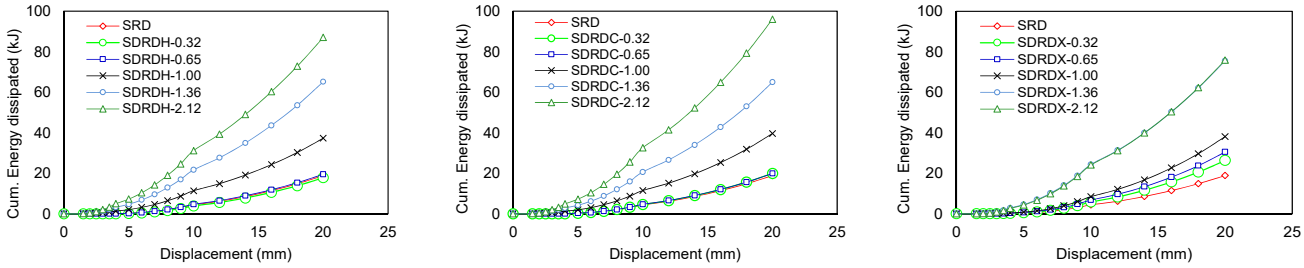

(a) SDRDH (b) SDRDC (c) SDRDX

Fig. 14 Comparison of cumulative dissipated energy curves of the parametric models

to SRD model and there are not observed significant changes in their capacity. Also, in these improved models, with increase of α (increase in the thickness of the inner ring), the ultimate capacity, stiffness during loading and unloading and enclosed surface in the hysteresis rings also increase (Figs. 12(a) and (b)). According to Fig. 12(c), the improved model SDRDX shows a different behavior with respect to the other models presented. This difference in behavior is due to the performance and yielding mechanism of the proposed model. In the improved model, the ultimate capacity is generally increased by increase of the parameter α.

6.2 Failure modes and yielding mechanisms

The yielding mechanism has been investigated to appraise the performance of the proposed dampers. Due to the fact that the performance of ring dampers is according to the position of bending plastic hinges, therefore, the capacity and energy absorption in this system depend on the number of bending hinges. Fig. 15 illustrates the failure shape and the location of the plastic hinges of SRD model. In this model, the locations of the bending hinges at the ring connections with the plates at the top/bottom of the ring are observed. Fig. 16 exhibits the failure mode and the location of the plastic hinges in SDRDH models. According to Fig. 16, in SDRDH models the mechanism of formation of plastic hinges varies based on the inner ring thickness. In SDRDH models, where $\alpha < 1$ (for example, model SDRDH-0.32), the plastic hinges are not formed at the inner ring. The non-participation of the inner ring in within the range $\alpha < 1$ is also seen in the final capacity and the force-displacement hysteresis diagram, which indicates a similar behavior in this damper (in this range) and SDR model.

On the other hand, for $\alpha \geq 1$, the yield mechanism occurs at both the inner and outer rings, which increases the capacity and energy absorption. Fig. 17 exhibits the failure mode and the location of the plastic hinges in SDRDC models. Also, presence of the vertical connection plates exhibits an average increase of 7% in the ultimate capacity of SDRDC improved dampers compared to SDRDH improved dampers.

In Fig. 18 the failure mode and location of the plastic hinges of SDRDX models are shown. In this model, there are some differences in behavior with respect to the other proposed models, so that the number of plastic joints formed is higher. Also, in this model for $\alpha < 1$ (for example, model SDRDX-0.32), plastic hinges are not formed at the inner ring. However, for values close to $\alpha < 1$, due to the number of plastic hinges formed in SDRDX models, these

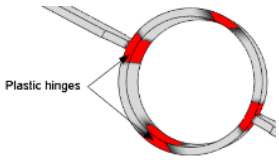

Fig. 15 Yielding mechanisms for SRD model

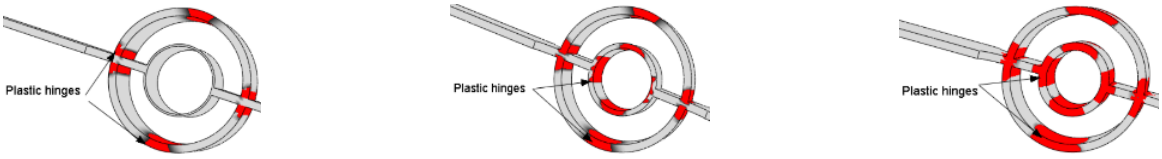

(a) $\alpha = 0.32$ (b) $\alpha = 1.00$ (c) $\alpha = 2.12$

Fig. 16 Yielding mechanisms for SDRDH models

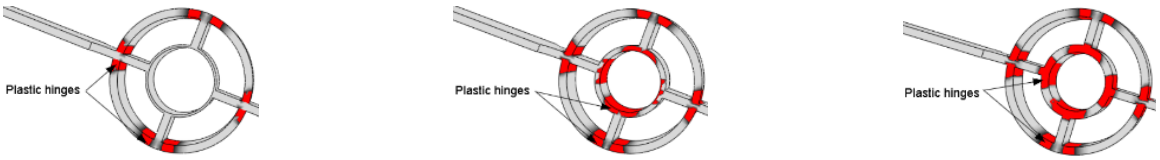

(a) $\alpha = 0.32$ (b) $\alpha = 1.00$ (c) $\alpha = 2.12$

Fig. 17 Yielding mechanisms for SDRDC models

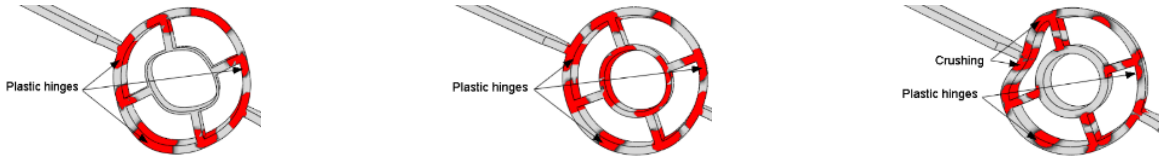

(a) $\alpha = 0.32$ (b) $\alpha = 1.00$ (c) $\alpha = 2.12$

Fig. 18 Yielding mechanisms for SDRDX models

models exhibit a higher ultimate capacity with respect to SDRDH and SDRDC models. In the proposed model of SDRDX, only at the diameter-to-thickness ratio of both rings being equal (α = 1), both the internal and external rings yield. On the other hand, for α > 1, the yield mechanism occurs in outer rings, which could be due to the high stiffness of the inner ring. Due to the fact that for values close to α > 1, the inner ring does not show any performance, therefore, at the ultimate capacity of dampers, SDRDX is not effective. On the other hand, due to the high stiffness of the inner ring, under loading of one side of the outer ring, crushing occurs at the connection with the end-plate (Fig. 18). Also, this stiffness limits the plastic rotations at the bottom and top of the outer ring.

7. Discussion and comparison of the improved models

Given that SDR model has been selected as the base model, evaluation of the improved models results based on Table 2, is as follows:

(i) Fig. 19 presents the plots of elastic stiffness (K_0) versus the α parameter for the base and improved models. The performance zone of the outer and inner rings is specified in the figures as well. α < 1 is indicative that the inelastic deformations develop only at the outer ring. The value of elastic stiffness depends on α ratio of the steel rings, so that by increasing the α parameter value of the steel rings, the elastic stiffness increases. The elastic stiffness of SDRDH, SDRDC, and SDSRX models were increased to 6%, 87%, and 82%, respectively, compared with SRD model.

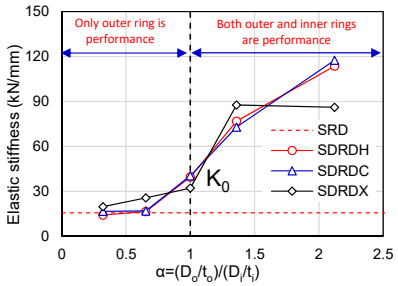

Fig. 19 Plots of elastic stiffness (K_0) versus α

(ii) Fig. 20 presents the plots of yield force (P_y) and ratio of yield force to weight (FWR) versus the α parameter for the base and improved models. SDRDH and SDRDC models, had similar performance, hence, there is negligible difference in their yield strength. Modifications to the yield strength against the parameter α in SDRDX model are different from SDRDH and SDRDC models, which are due to the type of performance and mechanism of plastic hinges formation. The yield force of SDRDH, SDRDC, and SDSRX models increased by 69%, 76%, and 66%, respectively, compared with SRD model.

According to Fig. 20(b) for values close to α < 1, in SDRDH and SDRDC models the value of the force-to-weight ratio is less than that of SRD model. Therefore, since the inner ring does not show performance in this range, it is not economically viable compared to SRD model. Also, for the mode where α = 1, the construction cost of SDRDH and SDRDC models is equal to that of SRD model. On the other hand, by increase in the parameter α, SDRDH and SDRDC models are very economical with respect to SRD model. The value of the yield force to weight ratio index in SDRDX models have increased compared to SDR model. This increase is on average 36%.

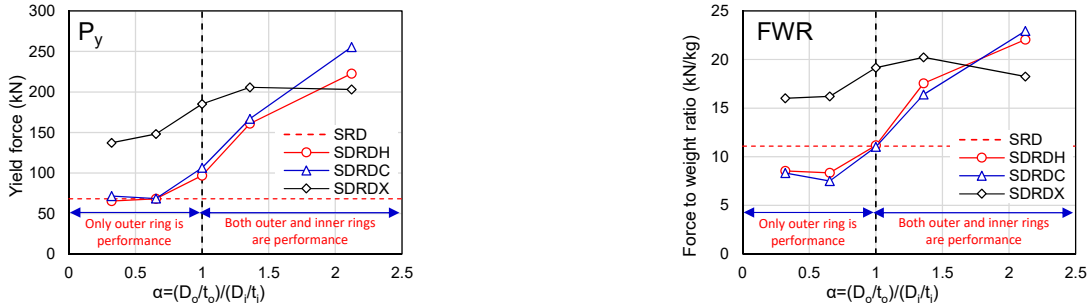

(a) (b)

Fig. 20 (a) Plots of yield force (P_y) versus α; and (b) plots of ratio of yield force to weight (FWR) versus α

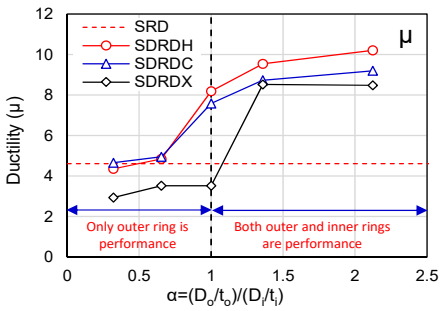

Fig. 21 Plots of ductility (μ) versus α

(iii) In the investigation of the performance, design, and analysis of the structure, the ductility parameter (μ) is implemented. For computing the ductility parameter, the peak displacement to the yield displacement ratio ($\mu = \delta_{max.}/\delta_y$) is utilized. The ductility parameter was estimated for the numerical models and the corresponding results are presented in Table 4. The ductility parameter means values have been calculated for the numerical model results, as well as variations of ductility parameter versus the α ratio are plotted in Fig. 21. As shown in Fig. 21, by enhancement in the D/t ratio in the steel inner ring, ductility increases, too. According to Fig. 21 in the range $\alpha < 1$, for SDRDH and SDRDC models, the value of the ductility parameter is equal to that of SRD model, which is due to the lack plastic hinges formation at the inner rings. For the state $\alpha = 1$, with formation of the plastic hinges at the inner ring, the ductility parameter in SDRDH and SDRDC models increased by an average of 41.5% compared to SRD model. For $\alpha > 1$, by enhancement in the D/t ratio of the inner ring, the ductility parameter in SDRDH and SDRDC models increased by 49% and 52%, respectively compared to SRD model. According to Fig. 21 in the range of $\alpha \leq 1$, for SDRDX model the ductility parameter decreases in comparison to SRD model. On the other hand, for the α <1 region, the value of the ductility parameter remains constant and increases by 46% compared to SRD model. This is due to the lack of plastic hinges at the inner rings and the crushing mechanism at the outer rings.

8. Conclusions

Studies performed on the steel RDs are confined to investigating the hysteresis behavior and energy dissipation. The results of studies performed on the steel RDs in CBF systems, demonstrated good ductility, high energy dissipation, and permanent hysteresis loops. On the other, these researchs were exclusived to a few test specimens with constant geometry and details of the RDs. Also, approachs were not adopted to progress the performance and efficiency of the steel RD. In this study, a number of methods are proposed to improve the hysteresis behavior and performance of steel RDs. For this purpose, a steel DRD is provided to implement in the CBFs systems. The cyclic behavior of the steel DRDs were examined applying the MFE method. The MFE models, the steel RD and DRDs with different construction details were developed for the parametric studies. MFE models were modeled and analyzed by a static general method, also the models were validated against the test results. In MFE modeling, the nonlinear behavior of geometrical and materials were considered in the study. In the parametric studies, the influence of the diameter to the thickness ratio of the inner ring, at the steel DRDs were investigated. The results of numerical studies included the load-displacement hysteresis curve, elastic stiffness, ultimate capacity, and total energy dissipation. The results exhibited that the diameter to the thickness ratio of the inner ring in the steel DRDs has a substantial influence on determining the hysteresis behavior, ductility, ultimate capacity and performance, as well as energy dissipation. Also, the results showed that the construction details of the internal and external ring connections have a considerable effect on the hysteresis behavior of the steel DRDs. According to the results of parametric studies, the optimal design and performance only have been observed in SDRDH and SDRDC models in the range $\alpha > 1$, which increases ductility, energy dissipation and ultimate capacity. Also, in these models, an increase in the yield force-to-weight ratio parameter, compared to the steel ring model, has been observed. This indicates a reduction in the construction cost and cost-effectiveness of these models. Also, selecting appropriate dimensions for the inner ring enhances the ductility and energy-dissipation of the steel DRDs.

References

ABAQUS-6.10 (2010), Standard user's manual. Hibbitt, Karlsson and Sorensen, Inc.

Abbasnia, R., Vetr, M.G.H., Ahmadi, R. and Kafi, M.A. (2008), "Experimental and analytical investigation on the steel ring ductility", *J. Sharif Sci. Technol.*, **52**, 41-48.

Aghlara, R., Tahir, M.M. and Adnan, A.B. (2018), "Experimental study of Pipe-Fuse Damper for passive energy dissipation in structures", *J. Constr. Steel Res.*, **148**, 351-360. https://doi.org/10.1016/j.jcsr.2018.06.004

AISC 360-16 (2016), American Institute of Steel Construction, Specification for Structural Steel Buildings (ANSI/AISC 360–16).

Andalib, Z., Kafi, M.A., Kheyroddin, A. and Bazzaz, M. (2014), "Experimental investigation of the ductility and performance of steel rings constructed from plates", *J. Constr. Steel Res.*, **103**, 77-88. https://doi.org/10.1016/j.jcsr.2014.07.016

ATC-24 (1992), Guidelines for cyclic seismic testing of components of steel structures.

Batterbee, D.C. and Sims, N.D. (2005), "Vibration isolation with smart fluid dampers: a benchmarking study", *Smart Struct. Syst., Int. J.*, **1**(3), 235-256. https://doi.org/10.12989/sss.2005.1.3.235

Bazzaz, M., Kheyroddin, A., Kafi, M.A. and Andalib, Z. (2012), "Evaluation of the seismic performance of off-centre bracing system with ductile element in steel frames", *Steel Compos. Struct., Int. J.*, **12**(5), 445-464. https://doi.org/10.12989/scs.2012.12.5.445

Bazzaz, M., Andalib, Z., Kheyroddin, A. and Kafi, M.A. (2015), "Numerical comparison of the seismic performance of steel

rings in off-centre bracing system and diagonal bracing system", *Steel Compos. Struct., Int. J.*, **19**(4), 917-937. https://doi.org/10.12989/scs.2015.19.4.917

Benavent-Climent, A. (2010), "A brace-type seismic damper based on yielding the walls of hollow structural sections", *Eng. Struct.*, **32**(4), 1113-1122. https://doi.org/10.1016/j.engstruct.2009.12.037

Bergman, D. (1987), Evaluation of cyclic testing of steel-plate devices for added damping and stiffness, Dept. of Civil Engineering, University of Michigan, MI, USA. https://www.worldcat.org/title/evaluation-of-cyclic-testing-of-steel-plate-devices-for-added-damping-and-stiffness/oclc/20751244

Chaboche, J.L. (1986), "Time-independent constitutive theories for cyclic plasticity", *Int. J. Plast.*, **2**(2), 149-188. https://doi.org/10.1016/0749-6419(86)90010-0

Chaboche, J.L. (1989), "Constitutive equations for cyclic plasticity and cyclic viscoplasticity", *Int. J. Plast.*, **5**(3), 247-302. https://doi.org/10.1016/0749-6419(89)90015-6

Chan, R.W.K. and Albermani, F. (2008), "Experimental study of steel slit damper for passive energy dissipation", *Eng. Struct.*, **30**(4), 1058-1066. https://doi.org/10.1016/J.ENGSTRUCT.2007.07.005

Chen, Z., Dai, Z., Huang, Y. and Bian, G. (2013), "Numerical simulation of large deformation in shear panel dampers using smoothed particle hydrodynamics", *Eng. Struct.*, **48**, 245-254. https://doi.org/10.1016/J.ENGSTRUCT.2012.09.008

Duan, Y., Ni, Y.Q., Zhang, H., Spencer, B.F., Ko, J.M. and Dong, S. (2019), "Design formulas for vibration control of sagged cables using passive MR dampers", *Smart Struct. Syst., Int. J.*, **23**(6), 537-551. https://doi.org/10.12989/sss.2019.23.6.537

Eldin, M.N., Kim, J. and Kim, J. (2018), "Optimum distribution of steel slit-friction hybrid dampers based on life cycle cost", *Steel Compos. Struct., Int. J.*, **27**(5), 633-646. https://doi.org/10.12989/scs.2018.27.5.633

Farghaly, A.A. (2015), "Seismic analysis of 3-D two adjacent buildings connected by viscous dampers with effect of underneath different soil kinds", *Smart Struct. Syst., Int. J.*, **15**(5), 1293-1309. https://doi.org/10.12989/sss.2015.15.5.1293

FEMA 356 (2000), Federal Emergency Management Agency, Prestandard and Commentary for the Seismic Rehabilitation of Buildings.

Gorji Azandariani, M., Abdolmaleki, H. and Gorji Azandariani, A. (2020a), "Numerical and analytical investigation of cyclic behavior of steel ring dampers (SRDs)", *Thin-Wall. Struct.*, **151**, 106751. https://doi.org/10.1016/j.tws.2020.106751

Gorji Azandariani, M., Gorji Azandariani, A. and Abdolmaleki, H. (2020b), "Cyclic behavior of an energy dissipation system with steel dual-ring dampers (SDRDs)", *J. Constr. Steel Res.*, **172**, 106145. https://doi.org/10.1016/j.jcsr.2020.106145

Gray, M.G., Christopoulos, C. and Packer, J.A. (2014), "Cast steel yielding brace system for concentrically braced frames: concept development and experimental validations", *J. Struct. Eng.*, **140**(4), 04013095. https://doi.org/10.1061/(ASCE)ST.1943-541X.0000910

Hsu, H.L. and Halim, H. (2017), "Improving seismic performance of framed structures with steel curved dampers", *Eng. Struct.*, **130**, 99-111. https://doi.org/10.1016/j.engstruct.2016.09.063

Hsu, H.-L.L. and Halim, H. (2018), "Brace performance with steel curved dampers and amplified deformation mechanisms", *Eng. Struct.*, **175**, 628-644. https://doi.org/10.1016/j.engstruct.2018.08.052

Kelly, J.M., Skinner, R.I. and Heine, A.J. (1972), "Mechanisms of energy absorption in special devices for use in earthquake resistant structures", *Bull. N.Z. Soc. Earthq. Eng.*, **5**(3), 63-88. https://www.nzsee.org.nz/db/Bulletin/Archive/05(3)0063.pdf

Kim, J., Kim, M. and Eldin, M.N. (2017), "Optimal distribution of steel plate slit dampers for seismic retrofit of structures", *Steel Compos. Struct.*, **25**(4), 473-484. https://doi.org/10.12989/scs.2017.25.4.473

Koetaka, Y., Chusilp, P., Zhang, Z., Ando, M., Suita, K., Inoue, K. and Uno, N. (2005), "Mechanical property of beam-to-column moment connection with hysteretic dampers for column weak axis", *Eng. Struct.*, **27**(1), 109-117. https://doi.org/10.1016/j.engstruct.2004.09.002

Kori, J.G. and Jangid, R.S. (2008), "Semi-active friction dampers for seismic control of structures", *Smart Struct. Syst., Int. J.*, **4**(4), 493-515. https://doi.org/10.12989/sss.2008.4.4.493

Li, H.-N. and Li, G. (2007), "Experimental study of structure with "dual function" metallic dampers", *Eng. Struct.*, **29**(8), 1917-1928. https://doi.org/10.1016/J.ENGSTRUCT.2006.10.007

Li, G.Q., Sun, Y.Z., Jiang, J., Sun, F.F. and Ji, C. (2019), "Experimental study on two-level yielding buckling-restrained braces", *J. Constr. Steel Res.*, **159**, 260-269. https://doi.org/10.1016/j.jcsr.2019.04.042

Mahjoubi, S. and Maleki, S. (2016), "Seismic performance evaluation and design of steel structures equipped with dual-pipe dampers", *J. Constr. Steel Res.*, **122**, 25-39. https://doi.org/10.1016/J.JCSR.2016.01.023

Maleki, S. and Bagheri, S. (2010a), "Pipe damper, Part I: Experimental and analytical study", *J. Constr. Steel Res.*, **66**(8), 1088-1095. https://doi.org/10.1016/j.jcsr.2010.03.010

Maleki, S. and Bagheri, S. (2010b), "Pipe damper, Part II: Application to bridges", *J. Constr. Steel Res.*, **66**(8), 1096-1106. https://doi.org/10.1016/j.jcsr.2010.03.011

Maleki, S. and Mahjoubi, S. (2013), "Dual-pipe damper", *J. Constr. Steel Res.*, **85**, 81-91. https://doi.org/10.1016/j.jcsr.2013.03.004

Maleki, S. and Mahjoubi, S. (2014), "Infilled-pipe damper", *J. Constr. Steel Res.*, **98**, 45-58. https://doi.org/10.1016/j.jcsr.2014.02.015

Mohammadi, M., Kafi, M.A., Kheyroddin, A. and Ronagh, H.R. (2020), "Performance of innovative composite buckling-restrained fuse for concentrically braced frames under cyclic loading", *Steel Compos. Struct., Int. J.*, **36**(2), 163-177. https://doi.org/10.12989/SCS.2020.36.2.163

Mohebkhah, A. and Azandariani, M.G. (2016), "Lateral-torsional buckling resistance of unstiffened slender-web plate girders under moment gradient", *Thin-Wall. Struct.*, **102**, 215-221. https://doi.org/10.1016/j.tws.2016.02.001

Nakashima, M. (1995), "Strain-hardening behavior of shear panels made of low-yield steel. I: test", *J. Struct. Eng.*, **121**(12), 1742-1749. https://doi.org/10.1061/(ASCE)0733-9445(1995)121:12(1750)

Oh, S.H., Kim, Y.J. and Ryu, H.S. (2009), "Seismic performance of steel structures with slit dampers", *Eng. Struct.*, **31**(9), 1997-2008. https://doi.org/10.1016/j.engstruct.2009.03.003

Qu, B., Dai, C., Qiu, J., Hou, H. and Qiu, C. (2019), "Testing of seismic dampers with replaceable U-shaped steel plates", *Eng. Struct.*, **179**, 625-639. https://doi.org/10.1016/J.ENGSTRUCT.2018.11.016

Rai, D.C., Annam, P.K. and Pradhan, T. (2013), "Seismic testing of steel braced frames with aluminum shear yielding dampers", *Eng. Struct.*, **46**, 737-747. https://doi.org/10.1016/J.ENGSTRUCT.2012.08.027

Sahoo, D.R., Singhal, T., Taraithia, S.S. and Saini, A. (2015), "Cyclic behavior of shear-and-flexural yielding metallic dampers", *J. Constr. Steel Res.*, **114**, 247-257. https://www.sciencedirect.com/science/article/pii/S0143974X15300547

Shi, Y., Wang, M. and Wang, Y. (2011), "Experimental and constitutive model study of structural steel under cyclic loading", *J. Constr. Steel Res.*, **67**(8), 1185-1197. https://doi.org/10.1016/j.jcsr.2011.02.011

Skinner, R.I., Kelly, J.M. and Heine, A.J. (1974), "Hysteretic dampers for earthquake-resistant structures", *Earthq. Eng. Struct. Dyn.*, **3**(3), 287-296. https://doi.org/10.1002/eqe.4290030307

Talebizadehsardari, P., Eyvazian, A., Gorji Azandariani, M., Nhan Tran, T., Kumar Rajak, D. and Babaei Mahani, R. (2020), "Buckling analysis of smart beams based on higher order shear deformation theory and numerical method", *Steel Compos. Struct., Int. J.*, **35**(5), 635-640. https://doi.org/https://doi.org/10.12989/scs.2020.35.5.635

Tsai, K., Chen, H., Hong, C. and Su, Y. (1993), "Design of steel triangular plate energy absorbers for seismic-resistant construction", *Earthq. Spectra*, **9**(3), 505-528. https://doi.org/10.1193/1.1585727

Vilela, P.M.L., Carvalho, H., Grilo, L.F., Montenegro, P.A. and Calçada, R.B. (2019), "Unitary model for the analysis of bolted connections using the finite element method", *Eng. Fail. Anal.*, **104**, 308-320. https://doi.org/10.1016/j.engfailanal.2019.06.001

Wang, C.L., Gao, Y., Cheng, X., Zeng, B. and Zhao, S. (2019), "Experimental investigation on H-section buckling-restrained braces with partially restrained flange", *Eng. Struct.*, **199**, 109584. https://doi.org/10.1016/j.engstruct.2019.109584

Whittaker, A.S., Bertero, V.V., Thompson, C.L. and Alonso, L.J. (1991), "Seismic testing of steel plate energy dissipation devices", *Earthq. Spectra*, **7**(4), 563-604. https://doi.org/10.1193/1.1585644

Xu, L.-Y., Nie, X. and Fan, J.-S. (2016), "Cyclic behaviour of low-yield-point steel shear panel dampers", *Eng. Struct.*, **126**, 391-404. https://doi.org/10.1016/J.ENGSTRUCT.2016.08.002

Yeh, C.H., Lu, L.Y., Chung, L.L. and Huang, C.S. (2001), "Test of a full-scale steel frame with TADAS", *Earthq. Eng. Eng. Seismol.*, **3**(2).

Zhang, C., Zhang, Z. and Shi, J. (2012), "Development of high deformation capacity low yield strength steel shear panel damper", *J. Constr. Steel Res.*, **75**, 116-130. https://doi.org/10.1016/J.JCSR.2012.03.014

Zhou, Z., Ye, B. and Chen, Y. (2019), "Experimental investigation of curved steel knee braces with adjustable yield displacements", *J. Constr. Steel Res.*, **161**, 17-30. https://doi.org/10.1016/j.jcsr.2019.06.011

BS